UNIVERSIDAD NACIONAL AUTÓNOMA DE MÉXICO

FACULTAD DE CIENCIAS

OPTICAL LEVITATION OF DROPLETS

WHISPERING GALLERY MODES, HARMONIC RESONANCE AND CHARGE QUANTIZATION

T E S I S

QUE PARA OBTENER EL TÍTULO DE:

FÍSICO

P R E S E N T A :

JAVIER TELLO MARMOLEJO

DIRECTOR DE TESIS:
DR. REMIGIO CABRERA TRUJILLO

Ciudad de México, 2019

This work was performed under the supervision of Professor Dag Hanstorp at the University of Gothenburg and with the financial support of the Linnaeus-Palme Foundation.

Resumen

Se llevaron a cabo tres experimentos con gotas de aceite de silicón levitadas ópticamente dentro de una cámara de vacío. El arreglo experimental permitía impulsarlas con un campo eléctrico y controlar la presión dentro de la cámara.

En el primer experimento se observó que gotas levitando a presiones por abajo de 1.0 mbar se evaporan exponencialmente con el tiempo. Durante el proceso de evaporación se observaron saltos periódicos a causa de resonancias con el láser usado para crear la trampa ótica que dependen del tamaño de la gota. Se llevó a cabo una medición absoluta del tamaño de la gota durante el proceso de evaporación. Se muestra que las resonancias están relacionadas con cambios en el diámetro de la gota del orden de la longitud de onda del láser.

En el segundo experimento a las gotas se les aplicó una fuerza con un campo eléctrico oscilatorio a diferentes presiones. Un efecto de resonancia armónica fue observado en la frecuencia de resonancia y un ajuste del comportamiento fue hecho usando el modelo del oscilador armónico amortiguado y forzado. El ajuste fue usado para calcular la rigidez de la trampa k. Este cálculo de k puede ser usado para calibrar trampas ópticas y fue comparado con otros métodos recientes y similares.

En el tercer experimento se muestra un ejemplo visual de la cuantización de la carga. Una gota atrapada en un campo eléctrico fuerte se mueve en pasos cuantizados al ganar o perder uno o algunos electrones. El control preciso de la carga fue lograda usando radiación alfa. El resultado es una versión moderna y de una sola gota del experimento de Millikan.

Algunos de los resultados que se presentan pueden ser usados en el salón de clases como demostraciones del oscilador armónico amortiguado y forzado en los regímenes de sobreamortiguación y amortiguación débil, así como de la frecuencia de resonancia y de la cuantización de la carga. La mayoría de estas demostraciones puede ser observada por los estudiantes a simple vista.

Abstract

Three experiments were performed on optically levitated silicone oil droplets inside a vacuum chamber. The experimental setup allowed the droplets to be driven by an electric field and to change the pressure inside the chamber.

In the first experiment, droplets trapped at pressures under 1.0 mbar were found to evaporate exponentially. During the evaporation process, periodical jumps where observed caused by morphologically dependent resonances with the trapping laser. An absolute measurement of the size was performed simultaneously to the evaporation and the appearance of the resonances. The resonances are shown to be related with changes of the droplet diameter of the order of the laser's wavelength.

In the second experiment, the droplets were driven with an oscillating electric field at different pressures. A harmonic resonance effect was observed at the resonance frequency, and a fit of the behavior was made using the Damped Driven Harmonic Oscillator (DDHO) model. The fit was used to calculate the trap stiffness k. This calculation of k can be used to calibrate optical traps and is compared with other recent, similar methods.

In the third experiment, a visual example of the quantization of charge is shown. A trapped droplet in a strong electric field moves in quantized steps as it gains or losses single or small multiples of electrons. The precise manipulation of the charge was achieved using alpha radiation. The result is a modern single drop version of the Millikan experiment.

Some of the results can be used as classroom demonstrations of the DDHO in the over- and underdamped regimes, the resonance frequency, and the quantization of charge. Most of these are visible for students by the naked eye.

Foreword

I started working on optical levitation at the University of Gothenburg in Sweden thanks to the Linnaeus-Palme exchange program. This thesis is, in a way, an account of my journey here and of all the amazing people that helped me along the way.

A little like the field of optical levitation itself, my project started with a simple goal and evolved into many different things. On top of that, it had both research and didactic interests from the start. Because of this, the contents ended up being quite broad. I can only say that I did my best to thread it all together and, if nothing else, it has taught me how new things can be found when you least expect them.

I enjoyed working at the University of Gothenburg, and I hope you enjoy reading about it.

Regards,

Javier

Contents

1 Introduction

A series of brilliant experiments starting in 1969 took Arthur Ashkin and Joe Dziedzic from a "back of the envelope" calculation to the optical trapping and "opticution" (death by light) of bacteria grown from Joe Dziedzic's ham sandwich [1]. Forty-nine years later Arthur Ashkin was awarded the Nobel Prize in Physics for "the optical tweezers and their application to biological systems" [2]. This thesis is based on their work and would be very different, if not impossible, without them.

As far back as the 17^{th} century, Johannes Kepler had already proposed the idea of radiation pressure to explain the orientation of comet tails [3]. Maxwell's Theory of Electromagnetism then gave a theoretical backbone to this idea [4], and at the start of the 20th century, Lebedev [5] was able to prove this experimentally. Nevertheless, the forces that could be brought onto macroscopic objects were so small that J. H. Poynting said about them "A very short experience in attempting to measure these forces is sufficient to make one realize their extreme minuteness — a minuteness which appears to put them beyond consideration in terrestrial affairs ..."[1]. The topic was then mostly forgotten until the 1960s, the decade when the laser was invented, and the first particle was optically manipulated.

Today the applications of Optical Manipulation (OM) are many more than just opticuting bacteria. In biology, it can be used to trap single cells [6] or to measure elastic and viscous properties of DNA solutions [7]. Other applications are to create nanomotors [8] or to investigate collisions between individual optically levitated droplets [9]. In atomic physics, OM led to the award of a Nobel Prize in 1997 to Steven Chu, Claude Cohen-Tannoudji and William D. Phillips "for development of methods to cool and trap atoms with laser light" [10].

For optical levitation in particular, some examples of applications include 3D force field microscopy [11], the search for kilogram-scale dark matter [12], and even juggling with light [13]. The interaction of the levitating objects with the light can also cause morphologically dependent resonances called Whispering Gallery Modes (WGM). These have themselves possible applications as biochemical sensors, mechanical sensors or filters [14].

The WGM were observed by Ashkin [15] and, more recently, were studied during the evaporation

of an optically levitated droplet [16]. The first experiment in this thesis shows the WGM caused by an exponential evaporation process of a levitated droplet. A correlation to an absolute measurement of the size was performed, and the resonances are shown to occur when the circumference is an integer multiple of the trapping light's wavelength.

Optical traps are usually modeled as harmonic potentials and, therefore, the movement of a trapped particle can be described by the differential equation of the Damped Driven Harmonic Oscillator (DDHO). The trap stiffness and damping coefficient, two important parameters in this equation, have been calculated previously for particles trapped in vacuum using electric fields [17, 18]. In the second experiment of this thesis, the resonance effect of a DDHO was observed by electrically driving levitating droplets in vacuum, and the measured resonance frequency was used to calculate the traps stiffness. Furthermore, a transition between the over- and under-damped regimes of the harmonic oscillator as the pressure drops is presented.

In 1913, Robert Millikan performed his famous oil drop experiment where he used a statistical analysis on many charged drops falling inside an electric field to calculate the charge of the electron [19]. The possibility of performing this measurement using optical levitation with a resolution higher than one elementary charge is mentioned by Ashkin et al. in [20] and has since been done using AC electric fields [21, 22]. In the third experiment of this thesis, a single drop Millikan experiment is presented where a levitating droplet inside a DC electric field shows visible quantized steps as its charge is changed by single elementary charges.

Finally, optical manipulation has been used with didactic purposes previously [23, 24]. The second and third experiments have very clear didactic applications. In the second one, the system is a fully manipulable harmonic oscillator where students can change the damping constant and driving force by turning a knob. Moreover, the resonance frequency can be found empirically on the spot and used to calculate the trap stiffness. Finally, in the third experiment, the single electron changes inside the droplet can be observed live or in a video, giving a visual example of the quantization of charge.

2 Theoretical Background

2.1 Optical Levitation

The basic principle for optical manipulation is the interaction between light and a dielectric particle. When its dielectric constant ϵ is different from that of the medium ϵ_0, the light passing through it will be refracted, causing an exchange of momentum between the light and the particle. The magnitude and direction of the added momentum will depend on the light intensity and geometry. Particular light beams can be chosen to produce forces that will translate, rotate, or even trap the particle. It is then of interest to calculate the forces that come from this interaction.

2.1.1 Lorenz-Mie regime

A complete way to calculate these forces is to use the Generalized Lorenz-Mie Theory [25]. It works for particles of any size and does not require the beam to be Gaussian. Nevertheless, it does depend on complicated expressions for the radiation pressure cross sections [26]. In order to avoid this, approximations for droplet diameters d a lot smaller or a lot bigger than the wavelength λ can be taken.

2.1.2 Rayleigh regime

For very small particles ($d << \lambda$) the Rayleigh approximation can be used. Here the particle is treated as a dipole in an electric field. This dipole will feel both a scattering force that pushes it along the direction of the laser and a gradient force that pushes it towards the point of maximum or minimum intensity.

A good example is the optical manipulation of atoms. In the presence of resonant light, the atom will absorb a photon and subsequently emit it spontaneously and isotropically. Every absorption will add momentum to the atom in the direction of the incident light, while the emissions will add momentum randomly in all directions that average out to zero. The sum of both processes results in the scattering force.

Concerning the gradient force, a neutral atom can be considered as a dipole with a polarizability α. The interaction of an electric dipole with a gradient electric field will result in a Lorenz force. It will

then push the atom towards the point of highest light intensity if $\alpha > 0$ or lowest light intensity if $\alpha < 0$. For atoms, α will change sign depending on whether the incident light is above or below the resonance frequency.

In general for a dipolar particle in the Rayleigh regime irradiated by an arbitrary monochromatic electromagnetic wave that varies slowly in space (paraxial) with angular frequency ω, it can be shown that the cycle averaged of the force is[27]

$$\langle F \rangle = \frac{\alpha'}{2} \nabla \langle |\mathbf{E}|^2 \rangle + \omega \alpha'' \langle \mathbf{E} \times \mathbf{B} \rangle \,, \tag{1}$$

where $|\mathbf{E}|$ is the time-dependent magnitude of the electric field vector, and α' and α'' are the dispersive (real) and dissipative (imaginary) parts of the polarizability $\alpha = \alpha' + i\alpha''$. In this equation the first term corresponds to the gradient force and the second one to the scattering force.

2.1.3 Geometrical regime

For large particles ($d >> \lambda$), such as the droplets levitated in this work, a geometrical approach can be used. This approach describes the electromagnetic field as rays that carry linear momentum p in the direction of propagation and of a magnitude inversely proportional to the wavelength $p = \frac{h}{\lambda}$. When a ray is refracted, absorbed or reflected by the particle, momentum is transferred and the same two main forces, scattering and gradient, arise.

When light is refracted on the surface of a spherical particle, the momentum of light changes and the conservation of momentum creates the forces shown in Fig. 1. In Fig. 1A the light gains momentum in the positive z direction. Hence the force felt by the droplet points down towards the focal point of the lens where the light intensity is the highest. In 1B the light gains momentum in the negative z direction. Hence the force felt by the droplet points up towards the focal point of the lens. Fig. 1C shows how a Gaussian beam profile generates a restoring radial force that pushes the droplet towards the center of the beam. These forces are the components of the gradient force that create a stable position in space. For optical tweezers, a very high numerical aperture lens is used in order to make the gradient force considerably stronger than the scattering force.

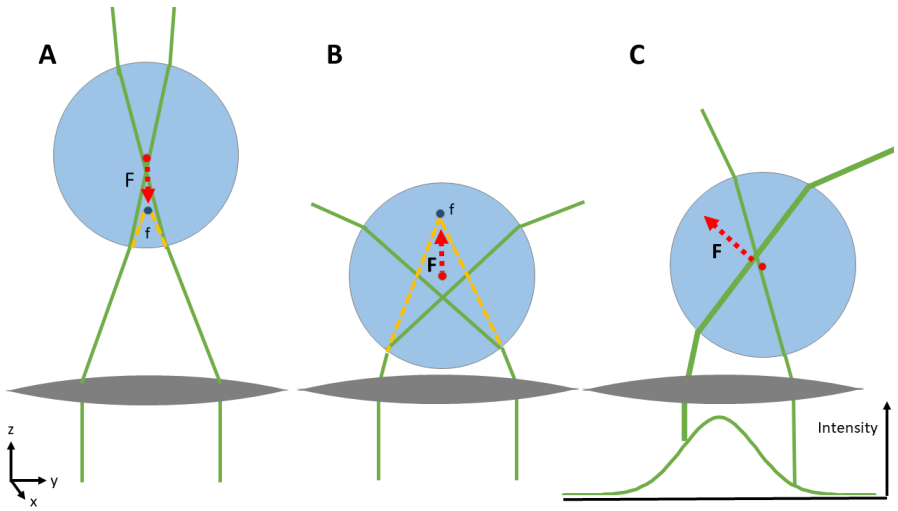

Figure 1: **A** For a droplet above the focal point the rays of light gain momentum in the positive z direction and the droplet is moved downwards. **B** For a droplet below the focal point the rays of light gain momentum in the negative z direction and the droplet is moved upwards. **C** A beam with a Gaussian profile will generate a restoring force towards its center.

On the other hand, when light is absorbed or reflected, it generates a radiation pressure in the direction of propagation given by

$$F_{scat} = Q\frac{n_0 P}{c}\,, \tag{2}$$

where n_0 is the refractive index of the medium, P is the power of the incident light, c is the speed of light, and Q is a dimensionless factor that accounts for the change in direction of the light. If the light passes straight through $Q = 0$, if it is absorbed $Q = 1$ and if it is reflected $Q = 2$. This value is somewhere between 0 and 2 and can be either measured experimentally or predicted theoretically.

Since optical levitation employs low numerical aperture lenses, the angle of incidence of the light is small, and the axial gradient force will be negligible compared to the scattering force. Fig. 2 shows a droplet being levitated by a vertical laser beam above the focal point. The higher the droplet is, the wider the beam and hence, the lower the laser power impacting the droplet. The droplet will also feel a gravitational force and an axially stable point exists where the gravitational and scattering forces are equal. Radially, the droplet will feel the same restoring force shown in Fig. 1C and a stable point in

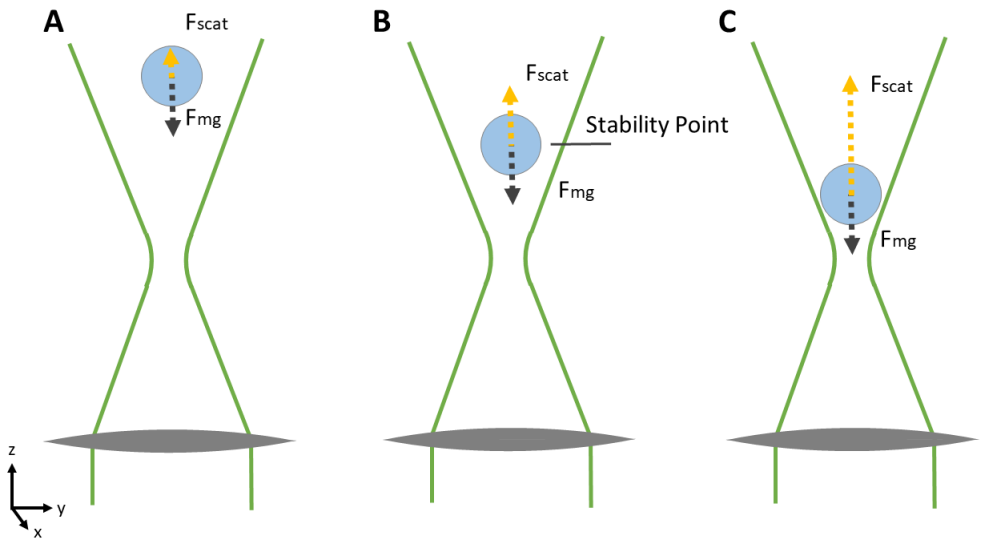

Figure 2: **A** Above the stability point the gravitational force is stronger than the scattering force. **B** At the stability point the gravitational and scattering forces are equal and the droplet is stable. **C**

Below the stability point the scattering force is greater than the gravitational force.

space is created.

It is worth mentioning that the discussion above considers a particle with a dielectric constant higher than that of its surrounding medium. In the opposite case, such as hollow spheres in water, the particles will be attracted to the points of lower intensity. Other beam profiles such as second order Bessel-Gaussian beams can then be used to trap these particles. This is analogous to the change in sign of the polarizability in the case of atoms.

Even when all these methods predict the forces acting on a given particle, the calculations commonly depend on parameters that either are not known with total precision or are prone to changes during an experiment. Examples are evaporating droplets or changes in the refractive indexes caused by temperature or the medium. For this reason, the forces are usually calibrated experimentally [17, 18, 28].

2.2 Diffraction Patterns

When coherent light interacts with objects of comparable size with its wavelength, it creates large diffraction patterns. These patterns can be measured and contain information about the object. Since the levitating droplets have a radius as small as 30 times the wavelength of the light, diffraction patterns appear. Two are of interest, the Airy pattern and the Double Slit pattern.

2.2.1 Airy Pattern

Airy patterns occur when light passes through a small circular hole or around a circular obstacle. A levitating droplet acts as an obstacle for the laser beam, creating a pattern shown schematically in Fig. 7B. Isaksson et al. [23] have used these patterns before to measure the diameter of the droplets.

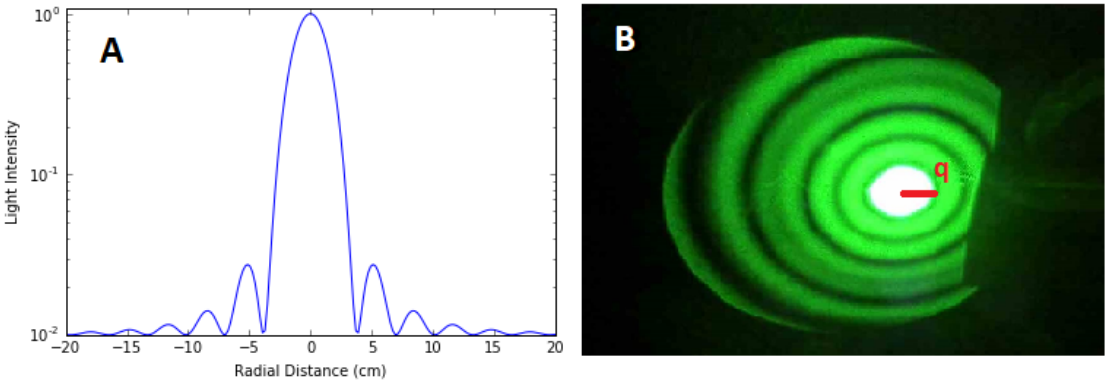

Figure 3: **A** Plot of Eq. (3) **B** Airy pattern produced by a levitating droplet.

The light intensity on a screen is given by

$$I(q) = I(0)\left[\frac{2J_1(kaq/R)}{kaq/R}\right]^2, \tag{3}$$

where $I(0)$ is the maximum intensity at the center of the pattern, q is the radial distance from the center, a is the radius of the hole, R is the distance between the object and the screen, $k = 2\pi/\lambda$ where λ is the laser light wavelength, and J_1 is the Bessel function of first order. Fig. 3A shows a plot of Eq. (3) while Fig. 3B shows a photograph of a pattern created by a drop. Note that Fig. 3A has a logarithmic

scale on the y axis for a better comparison with the photograph since the human eye senses brightness approximately logarithmically [29].

By measuring the radial distance q between the center and the middle of the first dark ring, the radius of the droplet a can be calculated by

$$a = \frac{1.22}{2}\frac{R\lambda}{q}\,. \tag{4}$$

2.2.2 Double Slit Pattern

The light scattered by a levitating droplet comes mostly from two points on the bottom and the top. The interference between the two sources will create a double slit diffraction pattern to the sides, as shown in Fig. 4. This approximation has been used previously by Lettieri et al. [30] to calculate the size of droplets. The radius a of the droplet will then be given by

$$a = \frac{2R\lambda}{S(2+\sqrt{2})}\,, \tag{5}$$

where R is the distance between the droplet and the screen, λ is the wavelength and S is the distance between two minima of light intensity on the screen.

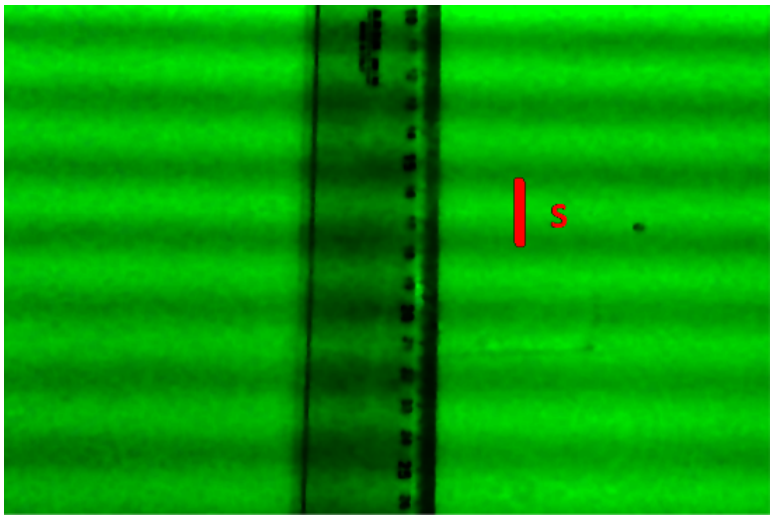

Figure 4: Diffraction pattern created by the droplet projected on the wall.

2.3 Trapping in Vacuum

The primary interest in using low pressures in this experiment is to control the damping of the system. The damping is caused by the viscous drag force of the fluid around the particle. According to Stoke's law this drag force, F_d, for a sphere will be

$$F_d = 6\pi\eta r v\,, \tag{6}$$

where η is the dynamic fluid viscosity, r is the radius, and v is the speed of the particle. The $6\pi\eta r$ term corresponds to the friction coefficient γ. We lower the value of the viscosity in the experiment by pumping out the air in the chamber.

The viscosity is independent of pressure down to a pressure p_0. This pressure corresponds to the point where the mean free path of the air particles is equal to the particle's diameter. Then, at pressures below p_0, the viscosity is found to fall linearly with the pressure [31].

The droplets reported here had diameters between 20 and 30 μm. For such particles, p_0 is about 3 mbar and we only expect to see a sufficient reduction of γ at a pressure of about or below 2 mbar.

Another effect of low pressures is a decrease in the thermal conductivity of air [32]. A droplet levitated by a laser beam will turn some of the laser's power into heat and then be cooled down by its surroundings. At high pressures, the cooling is fast enough, and the absorbed power low enough that we expect the droplet to stay at room temperature. However, when there are fewer air particles to collide with the droplet and remove some of its heat, the thermal conductivity of air is reduced, and the particle will heat up inversely proportional to the pressure [32].

2.4 Whispering Gallery Modes

In 1908 Gustav Mie published a solution to Maxwell's equations in which linearly polarized light is scattered by a homogeneous dielectric sphere [33], expanding on the work of Ludvig Lorenz and Albert Clebsch. At around the same time, Peter Debye published work on dielectric spheres but focusing rather on the radiating pressure created by the incident polarized light [34]. Together they formed what is now known as Lorenz-Mie-Debye theory.

With the advent of OM in the 1970s, these solutions became very relevant because most of the objects being manipulated were spherical and calculating the forces was extremely important. Nevertheless, lasers are not plane waves, and an expansion to the theory was needed. The solution for a general beam shape is now known as generalized Lorenz-Mie theory (GLMT).

One consequence of GLMT is a series resonances between the laser wavelength and the size of the sphere called Mie-Debye resonances or Whispering Gallery Modes (WGM) [16]. The process can be imagined in the following way. Some of the incident light will be able to overcome the centrifugal barrier around the sphere. Then it will come into it and reflect inside the sphere, leaking out some part at every reflection. When the path of the light is an integer multiple of the wavelength it will interact constructively; the particle becomes a resonant cavity and the scattering force increases. The optimal coupling between the modes and the incident beam occurs when the circumference is an integer multiple of the wavelength.

As the size changes, the internal reflection slowly increases or decreases, creating slow periodic changes in the scattering force. At resonance, the droplet becomes a resonant cavity, more of the light's momentum is absorbed, and the scattering force is greatly increased. As the size is continuously changing, the resonant size occurs only for a short moment. This results in a spectrum slow of periodic hills (coming from the slow increase in internal reflection) and fast spikes (coming from the resonance) on top. For a deeper explanation on WGM and numerical simulations of the spectra see [16, 33].

2.5 Charged Droplets in an Electric Field

A charged particle inside an electric field will feel a Coulomb force given by

$$F = qE\,, \tag{7}$$

where q is the charge of the particle and E is the magnitude of the electric field.

Liquid droplets coming from droplet dispensers or aerosols commonly have some amount of charge. Robert Millikan took advantage of this by comparing the falling speed of drops with and without a vertical DC electric field created by two parallel metallic plates [19]. This method allowed him to confirm

Faraday's idea of the quantization of charge and to measure the electron's charge.

The magnitude of the field produced inside a capacitor with a distance d between its parallel plates, and with a voltage difference V is given by

$$E = \frac{V}{d}\,. \tag{8}$$

2.6 Damped Driven Harmonic Oscillator

A harmonic oscillator is a system where any displacement from the equilibrium position creates a restoring force proportional to the displacement. This can be expressed as

$$m\frac{d^2y}{dt^2} = -ky\,, \tag{9}$$

where y is the position, m is the mass, and k is the spring constant. In the field of optical manipulation k is commonly referred to as the trap stiffness.

The system may also be subject to forces proportional and in opposite direction to the speed (damping) or external forces, F, (driving)

$$m\frac{d^2y}{dt^2} = -ky - 6\pi\eta r\frac{dy}{dt} + F\,. \tag{10}$$

The the undamped angular frequency w_0 is given by the mass and the stiffness as

$$w_0^2 = \frac{k}{m}\,, \tag{11}$$

where the angular frequency ω is related to the frequency f by $\omega = 2\pi f$. Therefore, dividing Eq. (10) by m and rearranging we obtain the DDHO differential equation

$$\frac{d^2y}{dt^2} + \gamma\frac{dy}{dt} + w_0^2 y = \frac{F}{m}\,, \tag{12}$$

where $\gamma = 6\pi\eta r/m$ is the friction coefficient.

An important case called a critically damped harmonic oscillator exists when $\gamma^2 - 4w_0^2 = 0$. When $\gamma^2 > 4w_0^2$ it is said that the system is over-damped and the solution will be a decaying exponential. When $\gamma^2 < 4w_0^2$ the system is under-damped, and the solution will be a sinusoidal wave multiplied by a decaying exponential. As long as $\gamma > 0$ both the over- and under-damped regimes eventually decay to the stability position, as shown in Fig. 5.

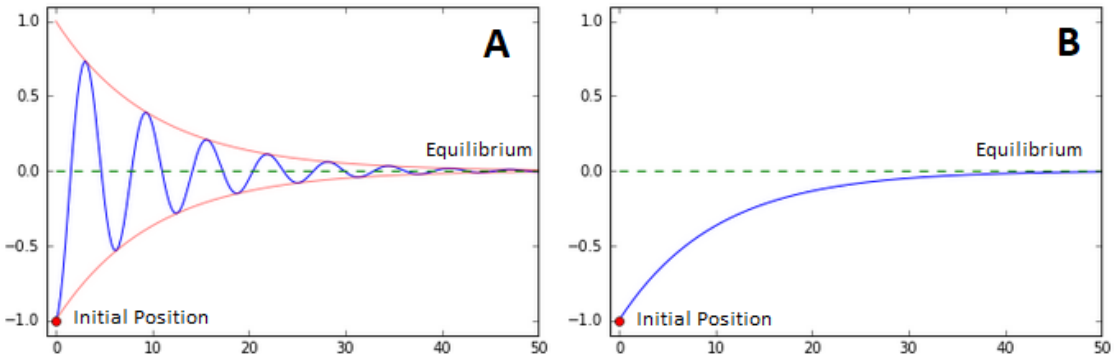

Figure 5: Decay to the equilibrium position of an **A** under-damped and **B** over-damped harmonic oscillator.

In the presence of external driving force, regardless of the system being over- or under-damped, after a long enough time, the initial conditions disappear and the system will follow the drive. In particular, if $F = F_0 sin(wt)$ then the solution will be

$$y = A(w, \gamma) sin(wt - \alpha)\,, \tag{13}$$

where w is the driving force frequency and α is the phase shift between the driving force and the oscillator given by

$$\alpha(w, \gamma) = \frac{\pi}{2} - arctan(\frac{w^2 - w_0^2}{\gamma w})\,. \tag{14}$$

The position in Eq. (13) will have a maximum when $wt - \alpha = n\pi/2$. Plugging Eq. (13) into Eq. (12) and looking at the time when the first maximum occurs, $n = 1$, we obtain

$$A(w, \gamma) = \frac{F_0}{m} \frac{sin(\frac{\pi}{2} + \alpha)}{w_0^2 - w^2}\,, \tag{15}$$

and normalizing by the amplitude at $w = 0$

$$\frac{A(w, \gamma)}{A_0} = \frac{sin(\frac{\pi}{2} + \alpha)}{1 - \frac{w^2}{w_0^2}}\,. \tag{16}$$

Fig. 6 shows plots of the amplitude of oscillation and phase shift of the system against the driving frequency w for different values of the friction coefficient γ. The values of γ are shown below each curve. Note how the curves become increasingly more sensitive to the change in damping as γ decreases.

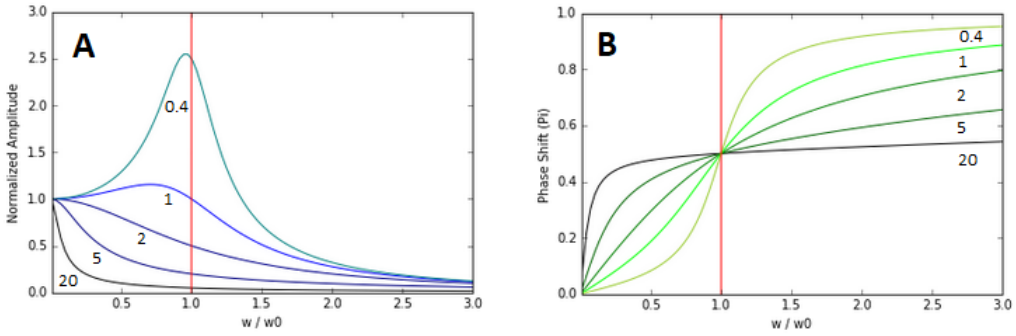

Figure 6: **A** Amplitude of oscillation response and **B** phase shift response for a damped driven harmonic oscillator. The numbers indicate the values of γ and the red line shows the resonance frequency where $w = w_0$.

3 Experimental Method

The three different experiments carried out on optically levitated silicone oil droplets are shown schematically in Fig. 7. This section describes the experimental setup and the methods used to perform each experiment. Fig. 7A schematically shows an evaporating droplet and the increase in scattering force that occurs when the circumference of the droplet is an integer multiple of the wavelength, that is, at a WGM. Fig. 7B shows the increase in amplitude of oscillation that happens for under-damped harmonic oscillator systems when a driving force with the resonance frequency is applied. Fig. 7C shows the expected displacement of a droplet sitting in a DC electric field when it absorbs or emits a single elementary charge.

The setup used to perform all three experiments can be seen schematically in Fig. 8. The droplets were levitated inside an aluminum vacuum chamber 60 mm high, 50 mm wide and 50 mm deep. A 532 nm CW linearly polarized laser (Laser Quantum gem532) with a beam diameter of 0.9 (1) mm is directed upwards into the chamber using a mirror and focused using a lens with focal length f of 100 mm. The length of the lens was chosen to have a low trap stiffness, making the drop move more per unit of force applied. This is particularly important for didactic purposes, since it allows students to see the oscillations by eye. However, lenses as short as 30 mm have been previously used in this setup to

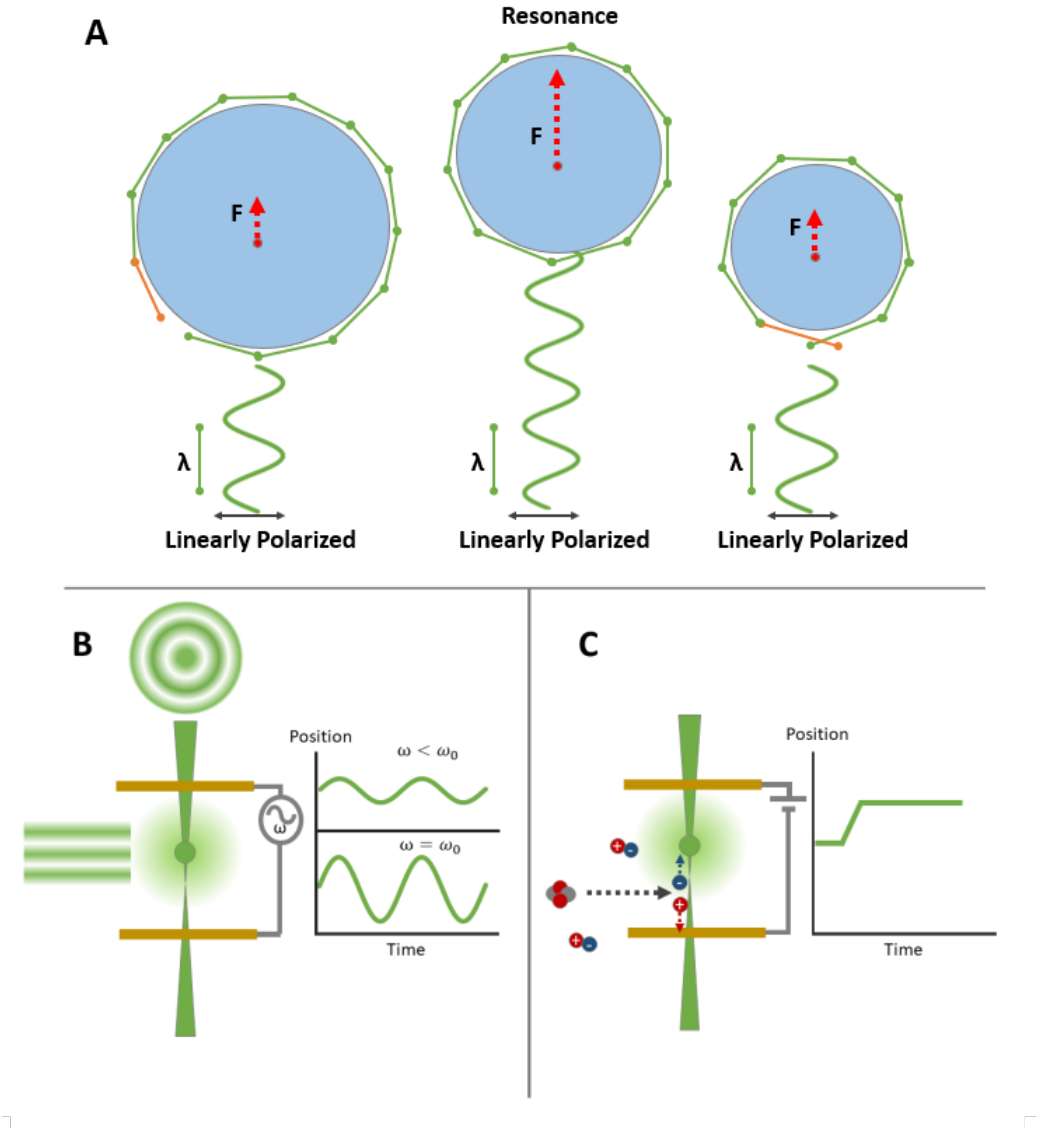

Figure 7: **A** Increase in the scattering force because of a WGM resonance for the droplet in the center. **B** Increase of the oscillating amplitude at the resonance frequency w_0. The scattered light creates an Airy pattern above and a double slit diffraction pattern to the side. **C** A levitating charged droplet in a DC electric field irradiated with alpha particles that change its charge. Elementary charge changes will create a step function shown to the right.

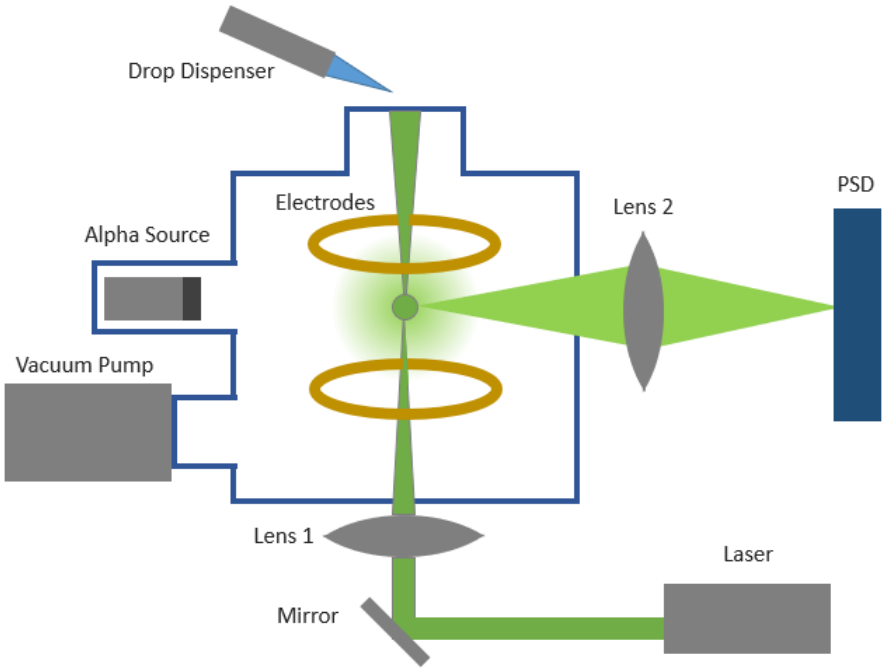

Figure 8: Experimental setup

successfully levitate droplets in stiffer traps [23]. The droplets were injected into the laser using a liquid micro-dispenser (GeSiM Bent Steel Capillary). The load in the dispenser consisted on a solution of 5 parts of isopropanol to 1 part of silicone oil.

After being focused, the diameter of the laser will decrease down to a minimum called the beam waist around the focal point and then expand again. The diameter of the beam waist is given by

$$2W_0 = \frac{4\lambda}{\pi}\frac{f}{D}, \tag{17}$$

where W_0 is the beam waist radius, λ is the wavelength of the laser, and D is the beam diameter before passing through the lens. Hence the beam waist in this setup had a diameter of $2W_0 = 75.2 \pm 8.4\mu m$. The diameter of the droplets never exceeded $30\mu m$, which means that the droplets always were inside the beam.

Two circular metallic plates, shown in yellow in Fig. 8, were used to create the electric field. The lower electrode was connected to a power supply capable of producing voltages of up to $\pm 1000V$. The upper electrode was connected to the ground. This means that for positive voltages the electric field

will point upwards. Therefore, applying a voltage is enough to know if the droplet has a net positive or negative charge. For example, a positive voltage will push positive droplets up.

The distances between the electrodes were different in different experiments. When the intention was to make the droplet oscillate and see the resonance frequency, then $d = 10\ mm$. On the other hand, to observe individual charges, a bigger electric field was needed and the distance was decreased to $d = 1\ mm$.

To control the pressure, the vacuum chamber is connected to a vacuum pump (Pfeiffer Vacuum DUO5M) through a variable leak valve (Leybold Gmbh DN 16 ISO-KF). The pressure can be set at any pressure between 980 mbar and 1×10^{-2} mbar using the valve, and a pressure gauge (Pfeiffer Single Gauge) was used to measure it.

3.1 Measurements

3.1.1 Position - Position Sensitive Device

As a droplet is levitated inside the chamber, it scatters laser light all directions. It can be recognized as the bright spot in the center of Fig. 9A. This light is then collected by Lens 2, as shown in Fig. 9B, which then produces an image on the Photo Sensitive Device (PSD). The lens's magnification M is given by

$$M = -\frac{b}{a}\,, \tag{18}$$

where a is the distance from the droplet to the lens and b is and the distance from the lens to the PSD. In this setup the magnification is $M = -5$.

In this case, a 1D interpolating readout PSD was used. It consists of a long photo-diode that creates a different current on the contacts connected to either end depending on where the incident light strikes the detector [38]. The distance of the spot of light from the center of the PSD d can be calculated using the output currents of the PSD I_A, I_B and the length L of the photo-diode

$$d = \frac{L}{2}\frac{I_B - I_A}{I_A + I_B}\,. \tag{19}$$

The lens magnifies not only the size but also the movement of the drop. The PSD has a length of 20 mm. Therefore, it has a measuring range of 4 mm and the real vertical displacement of the droplet will

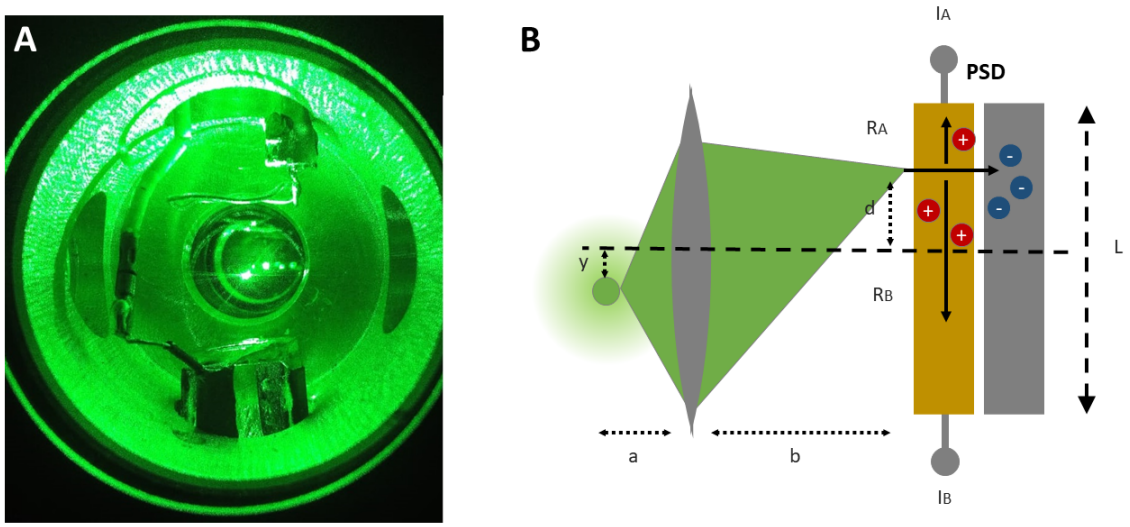

Figure 9: **A** The small bright spot visible by the bare eye inside the vacuum chamber is the levitating silicone oil droplet. **B** An image of the droplet on the PSD creates currents I_A and I_B from which the vertical displacement d can be calculated.

be

$$y = \frac{d}{|M|}\,. \tag{20}$$

The resolution is limited by the electrical noise inside the photo-diode and thermal movements of the particle in the trap. This noise was of around 0.004 mm.

3.1.2 Stiffness and Charge - Power Method

Consider a droplet levitated in an optical trap. At the stability point, the scattering force from Eq. (2) is equal to the gravity force

$$F_{scat1} = F_{mg}\,. \tag{21}$$

Increasing the laser power will raise the equilibrium position of the drop. If it is pushed down to the initial position with the electric field then

$$F_{scat2} = F_{mg} + F_E\,, \tag{22}$$

$$F_E = F_{scat2} - F_{mg} = F_{scat2} - F_{scat1}\,. \tag{23}$$

Since at both instances the position of the droplet is the same, the Q factor from Eq. (2) will be the same. Multiplying by $1 = F_{mg}/F_{scat1}$ we obtain

$$F_E = \frac{F_{scat2} - F_{scat1}}{F_{scat1}} F_{mg}\,, \tag{24}$$

and using Eqs. (2) and (8) we find the absolute charge

$$q = \frac{1}{E}\frac{\frac{QP_2}{c} - \frac{QP_1}{c}}{\frac{QP_1}{c}} mg = \frac{d}{V}\frac{P_2 - P_1}{P_1} mg\,. \tag{25}$$

Moreover, the displacement is linear to the force. Therefore the displacement from the initial position Δy will be related to the force needed to return it to zero F_E by Eq. (11). Then

$$k\Delta y = F_E = \frac{F_{scat2} - F_{scat1}}{F_{scat1}} F_{mg}\,, \tag{26}$$

and

$$k = \frac{P_2 - P_1}{\Delta y P_1} mg\,. \tag{27}$$

Here, Eqs. (25) and (27) give the absolute charge and the trap stiffness along the direction of the laser.

3.1.3 Whispering Gallery Modes

To observe the WGM, it was enough to trap a droplet and reduce the pressure. They usually appeared at some pressure below 1.0 mbar. Once the resonances were seen, the pressure was kept stable and the movement of the droplet was recorded. At the same time, a video of the diffraction pattern on the wall was taken to measure its size.

3.1.4 Oscillation Resonances

For this experiment, a droplet was trapped and made to oscillate by applying an AC electric field. The frequency was varied using a function generator and the oscillations recorded. Frequency sweeps from 0.05 rad/s to 60 rad/s were performed at pressures ranging from 980 mbar to 10^{-1} mbar.

A python program calculated the amplitude and frequency of each oscillation as well as the phase shift between each oscillation and the electric field. The program plotted the amplitude and the phase shift against the frequency for each oscillation.

3.1.5 Elementary Charge Differentials

A huge amplification of the electric force was needed to observe the quantization of charge. To do this, the electrodes were moved closer to a separation of only 1.0 mm. A droplet was trapped in between and made to oscillate with a small AC electric field. The alpha particle source was placed near it in order to reduce its absolute charge, which could be observed as a reduction in oscillating amplitude. Then, the magnitude of the electric field was increased, and the process repeated until the absolute charge was close to zero. This allowed the use of very high DC voltages without the droplet moving too far from the center of the electrodes.

We know that the displacement y will be proportional to the force and inversely proportional to the stiffness. For a change in charge q, with a given trap stiffness k and electric field $E = \frac{V}{d}$, this displacement is given by

$$y = \frac{Eq}{k} = \frac{Vq}{dk}\,. \tag{28}$$

For a voltage of 500 V, a typical trap stiffness of 5 nN/m and a distance between the electrodes of 1 mm, a change of a single elementary charge inside of the droplet would cause a displacement on the order of 0.02 mm, according to Eq. (28).

To change the charge inside the drop, a ^{241}Am radiation source was used. It has a half life of 432.2 years and produces both alpha and gamma radiation [36]. The gamma radiation has an energy of 59.54 keV and the most common alpha radiation has an energy of 5485.56 keV [37]. Both have sufficient energy to ionize the air molecules around the droplet or the molecules inside the drop.

The linear energy transfer as a function of distance traveled for charged particles follow the Bragg curve. This curve has a sharp peak at the end, after which the particles will very rarely ionize the medium. In the case of alpha radiation from ^{241}Am in air, the peak is at a distance about 4cm. By simply moving the source closer or further away from the droplet, it is possible to control the rate of ionization on the droplet.

As mentioned above, the alpha particles can hit the droplet directly and ionize it. Nevertheless, the droplet is very small, and it is far more likely for the alpha particle to ionize the air around it. The electrons and the positive molecules will then feel the force of the electric field, move vertically, and possibly hit the droplet, as shown in Fig. 7C.

The energy in one alpha particle coming from a ^{241}Am decay is enough to ionize around 4×10^5 oxygen atoms. If the purpose is to manipulate the charge of the droplet by single elementary charges, the number of ionizations would be huge. Nevertheless, most of the collisions happen on the way to the droplet, and not all the charges created will hit the drop. When the source is placed at the appropriate position, only a couple of charges will collide with it at a time.

4 Results and Discussion

4.1 Whispering Gallery Modes

This section presents results regarding the WGM in relationship with absolute measurements of size, and stability position of the droplet as it evaporates at low pressures.

4.1.1 Results

At pressures below 1.0 mbar, a periodic change in the stability position starts to appear on previously stable droplets. Each individual pattern consists of a wide hill followed by a narrow one, both with a spike near their tops and ending with a single spike in a valley. In Fig. 10 red vertical lines were drawn to separate each individual pattern. The shape of this hills and spikes coincides qualitatively to a Mie-Debye resonance spectrum [15].

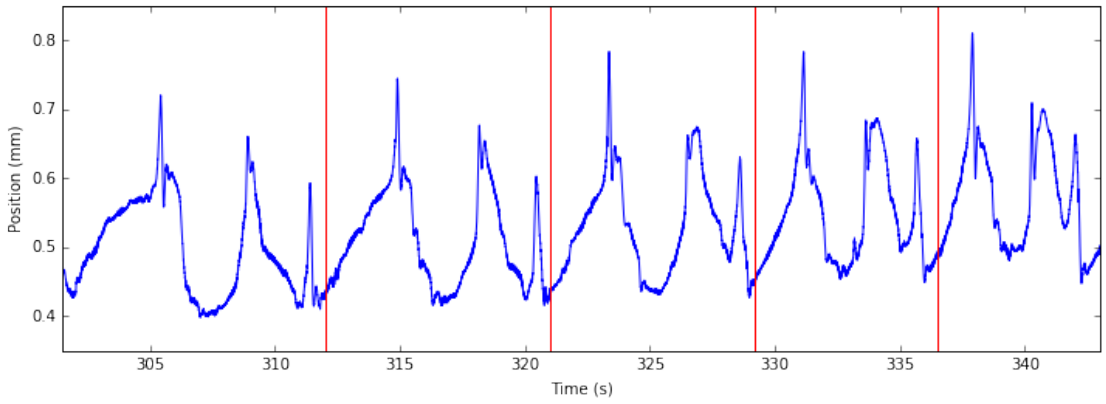

Figure 10: Periodic movement of a levitated droplet at 0.1 mbar.

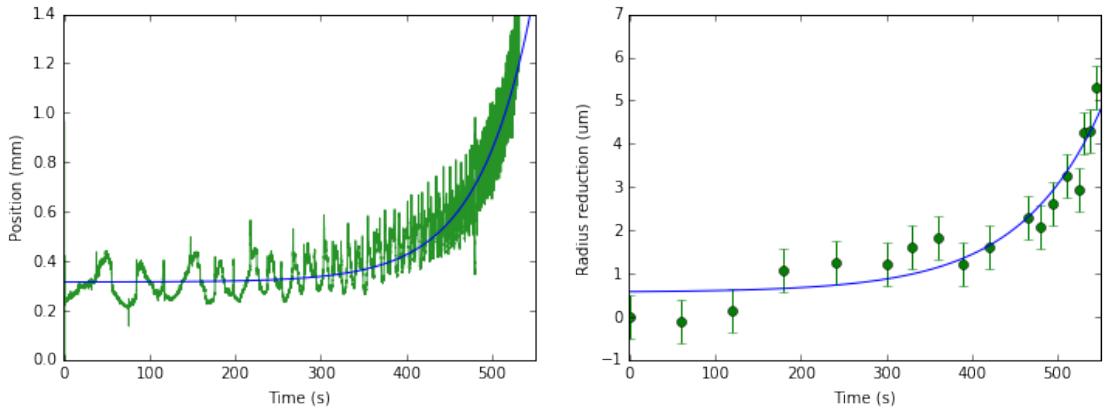

Figure 11: Evaporation of an optically levitated silicone oil drop. The recording of the position (left) shows the Mie-Debye resonances and the exponential increase in the stability position. The reduction in radius measured using a video of the diffraction pattern (right) shows an exponential increase too.

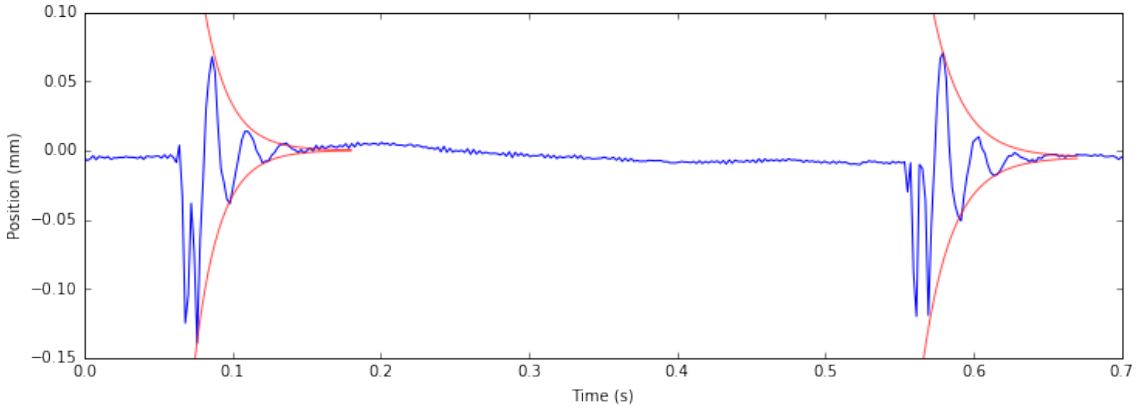

Figure 12: Under-damped oscillations of a levitated droplet at 0,8 mbar resulting from periodic excitations.

The left hand side of Fig. 11 shows the same recording as in Fig. 10, but on a longer time span. It reveals an exponential increase in the equilibrium position as well as an accelerating appearance of the resonances. Absolute size measurements were taken simultaneously with a video of the double slit diffraction pattern on the wall. The reduction in radius of the droplet was calculated and plotted in the right hand side of Fig. 11. By the end of the measurement, the stability position of the droplet increases rapidly, and suddenly the droplet disappears.

Every time there is a sharp spike, the droplet is moved from its stability position, and we would expect it to show an under-damped harmonic oscillator behavior as the one plotted in Fig. 5. This is clear in Fig. 12 where the resonances are especially strong and thus the oscillations especially visible.

4.1.2 Discussion

The change in size in Fig. 11 is evidence that the droplet is evaporating continuously. Every time the droplet reaches a certain size, the resonances appear. The evaporation seems to follow an exponential curve and therefore, the fitting of the data on both the right and left hand side of Fig. 11 was done with the following function

$$y = Ae^{Bt} + C\,. \tag{29}$$

Since A and C account for the scale and offset, each set of data gave a different fit for the A and C values, but the values for B are, as expected, similar to one another since the time evolution is the same. $B_{position} = 0.014368(24)s^{-1}$ and $B_{size} = 0.0104(27)s^{-1}$ with a percentage error between them of 27.6%. The percentage error stems in part from the measurements of the size. There are few points and they have a large uncertainty that carries on to B_{size}. A way to decrease the uncertainty of B_{size} would be to implement an image recognition program to calculate the size in every frame and thus have more points.

The similarity between $B_{position}$ and B_{size} indicates that the increase in height is proportional to the reduction in radius. To explain this, we see that the gravitational force depends on the mass, which decreases cubically with the radius. On the other hand, the scattering force depends on the height of the droplet and on the cross area of the sphere, which decreases quadratically with the radius. At the stability position the net force is zero, then

$$0 = F_{total} = F_{scatter} - F_{grav} = k_1 r^2 y - k_2 r^3 \,, \tag{30}$$

$$y = k_3 r \,. \tag{31}$$

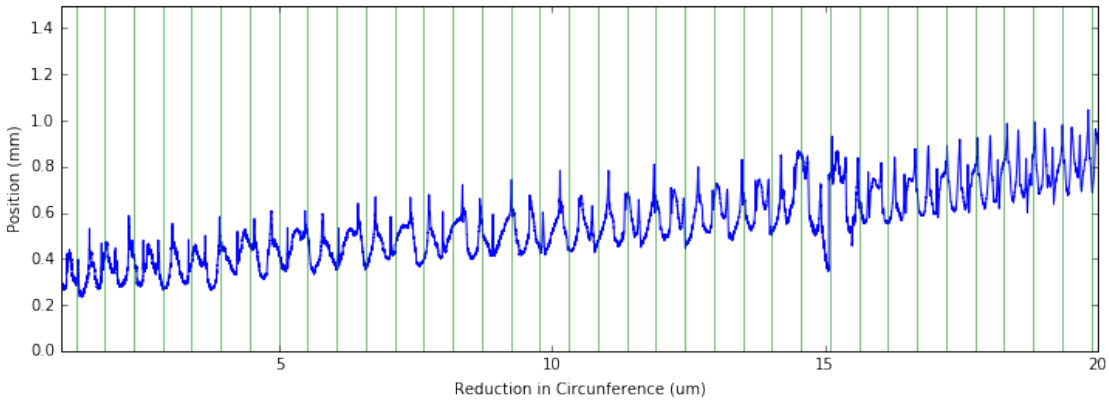

Figure 13: Mie-Debye resonances as a function of size. The vertical lines show changes of 532 nm in the droplet circumference.

Plotting the movement of the droplet against the change in circumference turns the exponential increase to a linear one, shown in Fig. 13. This also equalizes the distance between the resonances. The vertical lines were drawn every 532 nm. It can be seen that the pattern repeats itself around every two

multiples of 532 nm and that one out of three periodic resonances match the lines, particularly between 11 s and 16 s. Therefore some resonances seem to be indeed happening every time the diameter becomes a multiple of the wavelength. On the other hand, there seem to be more resonances than one every 532 nm, which could be caused by other resonance modes. It is also possible that the relevant distance is not the laser wavelength $\lambda = 532\ nm$ but the wavelength inside the drop, since the resonance happens inside it. The droplet has a refractive index of 1.405, therefore, comparing with changes of $\frac{\lambda}{1.405} = 378.65\ nm$ might also yield a correlation.

Nevertheless, it can be seen that the resonances in Fig. 13 are more closely spaced around a radius reduction of 18 μm than around a reduction of 10 μm. This probably stems from an insufficiently precise exponential fit for the radius reduction in Fig. 11. A more and more precise measurements of the absolute size of the droplet during the evaporation process could give a better measurement of the size dependence of the resonance modes.

4.2 Harmonic Resonance

The following section presents the oscillation resonance effect of an optically levitated silicone oil droplet at low pressures and discusses its possible application on the calibration of optical traps.

4.2.1 Results

Fig. 14 shows a typical frequency sweep at 1 atm. To the left, the electric field (blue) and the position of the droplet (green) are shown. The data was recorded with an acquisition rate of 500 points per second. To the right, the amplitude (blue) and phase shift between the driving force and the position (green) are shown. The data to the right was obtained from the one to the left, as described in section 3.1.4. All the data points for the amplitude were divided by the first one to give the normalized amplitude.

As expected for a highly damped driven harmonic oscillator, the amplitude of oscillation decays rapidly when the driving frequency is increased. On the other hand, the phase shift between the driving force and the motion increases fast at first and then very slowly. The resonance frequency is the point where the shift is $\frac{\pi}{2}$ but there is no increase in the amplitude.

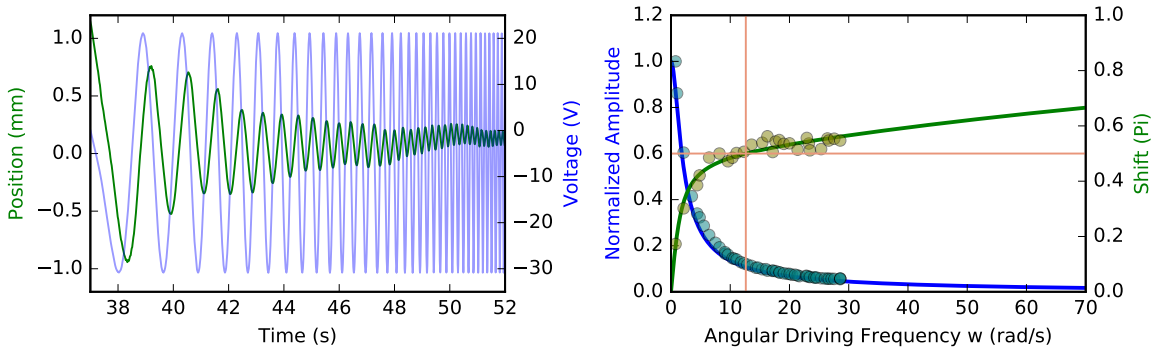

Figure 14: Frequency sweep at 980mbar

The fits of the curves on the right for the amplitude A and the shift α were made using Eqs. (14) and (16) respectively. Both equations depend on the same two parameters, the undamped angular resonance frequency w_0 and the friction coefficient γ. The fitting was done using the same pair of parameters for both fits. The red vertical line represents the value of w_0 obtained from the fit. The red horizontal line marks $\frac{\pi}{2}$ on the phase shift scale. Note how the red lines meet on top of the green phase shift line. This means that the resonance frequency value resulting from the fit coincides with the shift having a value of $\frac{\pi}{2}$, as is expected from Eq. (14).

The following Figs. 15 – 18 show frequency sweeps as the pressure is reduced. The behavior is similar until 0.68 mbar (Fig. 17), where a small increase in the amplitude can be observed at 24 rad/s. Note how the increase occurs to the left of w_0 as shown theoretically in Fig. 6A. The resonance is even more dramatic at 0,3 mbar (Fig. 18) where the amplitude increases by a factor of 2.5 and occurs closer to w_0. For both of these, the same "s" shape in the shift plot can be seen as in the low damping curves of Fig. 6B.

Using Eq. (11) we can use the value of w_0 given by the fit together with the mass calculated from the diffraction pattern to obtain a value for the trap stiffness. As a representative case, we will take the fit of Fig. 17. The procedure described in 3.1.2 gives a stiffness of $k_{power} = 4.10(60) nN/m$.

The fit gives $\gamma = 24.59(82)\ s^{-1}$ and $w_0 = 30.26(23)\ rad/s$. This droplet produced an Airy pattern with $q = 7.746(20)\ cm$ and hence had a radius of $10.72(21)\ \mu m$ and a mass of $5.01(17) \times 10^{-12}\ kg$. The

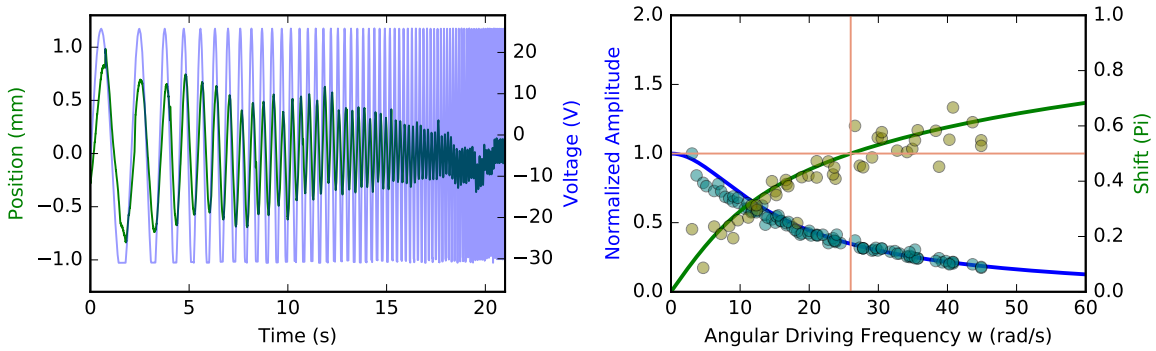

Figure 15: Frequency sweep at 9,1mbar

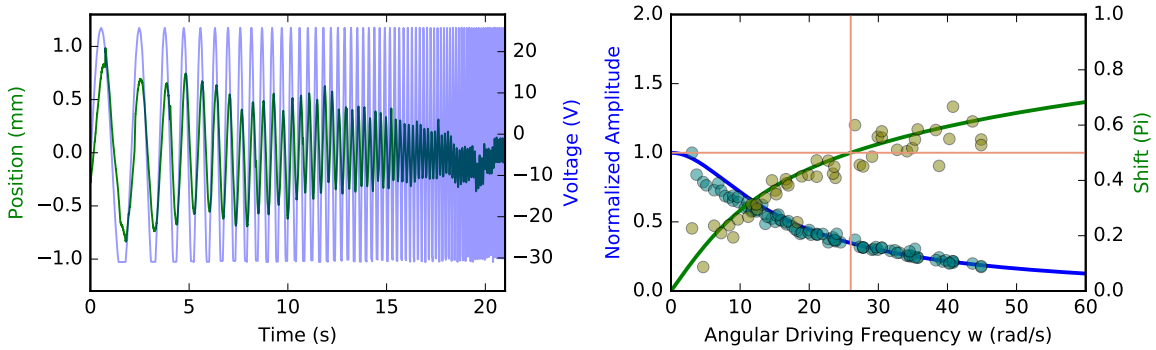

Figure 16: Frequency sweep at 2,5mbar

resulting trap stiffness is $k_{resonance} = 4.59(16)\ nN/m$. The trap stiffness obtained with the resonance method $k_{resonance}$ lies inside the error range of k_{power} and has an uncertainty almost 4 times lower.

4.2.2 Discussion

The frequency sweeps for low pressures show that it is possible to create a resonance effect on a levitating droplet. On the left hand side of these figures, we can see that the oscillations can be as big as 4 mm peak to peak, which makes the resonance visible with the naked eye.

Moreover, the evolution of the amplitude plots shows the transition between the over- and under-damped regimes of the DDHO. Comparing these plots qualitatively to the theoretical predictions in Fig. 6 it can be concluded that Figs. 14 and 15 show the over-damped behavior, Fig. 16 shows critical damping, and Figs. 17 and 18 show the under-damped behavior.

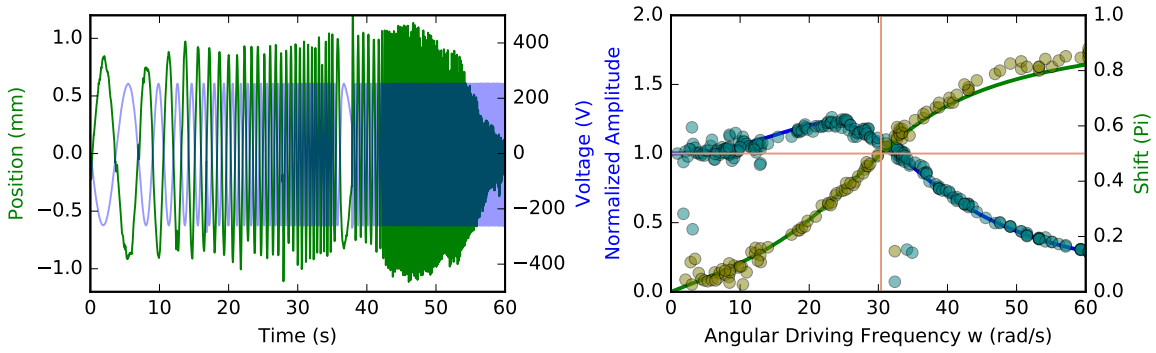

Figure 17: Frequency sweep at 0,68mbar

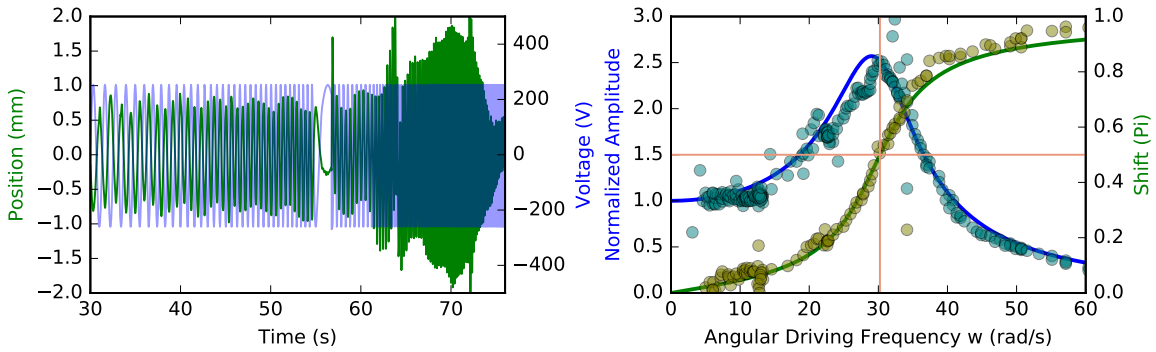

Figure 18: Frequency sweep at 0,3mbar

Turning now to the calculation of the trap stiffness, we have measured it using two different methods and found that the two methods give values that agree with their uncertainties, and that the frequency sweep method gives a smaller uncertainty. It would also be possible to apply the frequency sweep method with a horizontal electric field to measure the transverse stiffness instead of the axial stiffness. This measurement cannot be done with the laser power method.

A precise measurement of the trap stiffness and the friction coefficient is very dependent on small changes of pressure or size and temperature of the drop. It is therefore of interest to be able to calculate these values in a fast, repeatable and in situ manner. There are many calibration techniques currently being used to find the stiffness of optical trapping systems. Some examples are the Drag-force, Power Spectrum, Equipartition Theorem, and Time of Flight methods [28].

Nevertheless, to use these, it is usually necessary to know the fluid viscosity or temperature beforehand,

as well as the particle radius. In addition, these other methods normally depend on the presence of a surrounding fluid and a value for its friction coefficient, on knowledge of the temperature inside the particle (which might not be constant if the particle is being heated by the laser) or on very high position resolution.

To find the trap stiffness from the resonance frequency method, knowledge of the mass is sufficient. The measurement can be as fast as the ones mentioned above (around 1 minute) and can be done on relatively unstable particles or with low position resolution because of the increase of the signal to noise ratio that occurs at resonance.

Two other similar methods of calibration in vacuum have been reported. Park et al. [17] calculated the trap stiffness by averaging out a series of oscillations that resulted from individual delta excitations. The advantages of the resonance frequency method compared to Park et al.'s method [17] are that, since the effects are amplified during resonance, the averaging of many trajectories is not needed and it does not depend on the relaxation time, which could be high for traps with lower stiffness.

The other method used by Hebestreit et al. [18] applied a harmonic driving force with three different frequencies on a particle whose motion was cooled down using a feedback loop on the levitating laser. A fit of the power spectrum from the resulting oscillations gives the friction coefficient (related to the feedback cooling, not to the medium), the resonance frequency, and a calibration factor for the apparatus. The advantages of the resonance method over Hebestreit et al.'s method [18] are that no feedback cooling is needed and that the resonance can be observed in situ. Moreover, by applying a cooling system, the friction coefficient obtained is related to the cooling, while in our method the friction coefficient obtained is related directly to the viscosity of the medium.

Figs. 17 and 18 show many points outside of the fit. These points arise from WGM jumps that start occurring at such low pressures. These points are outliers and were not taken into account for the fits.

4.3 Elementary Charge Differentials

The following is a description of a method with which it is possible to observe the quantization of the electron and to manipulate the charge inside a levitated droplet with a precision of a couple of elementary

charges. The applications of precise measurement and control of charge are discussed.

4.3.1 Results

As explained in section 3.1.5, a levitated droplet was discharged, moved to a new equilibrium position with a powerful 660 V DC electric field, and its charge was manipulated using an alpha source. The result is the step function shown in Fig. 19. The distance between the horizontal lines marks the expected displacement from a single elementary charge differential. The lines were fitted to have the best coincidence with the steps and have a distance between them of 0.0186 mm. The calculated expected size of the steps from Eq. (28) is of 0.0211 (21). The values have a percentage error of 11.8%.

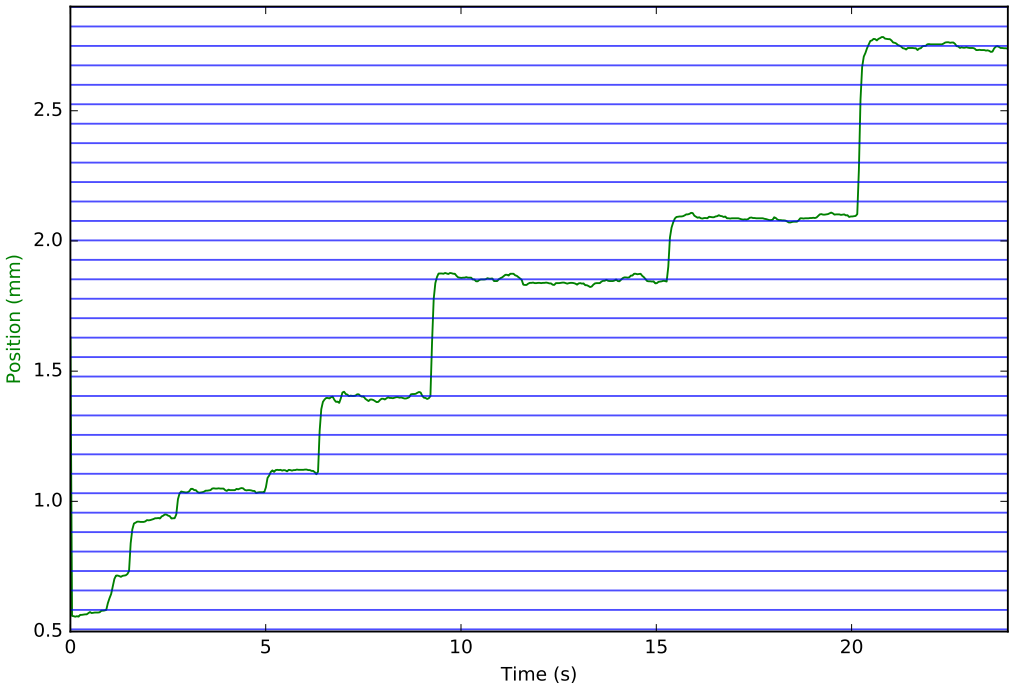

Figure 19: Visualization of the quantization of charge. The green line shows the displacement caused by small multiples of single elementary charge differentials of a droplet inside an electric field. Each blue horizontal line represents the expected displacement by a single elementary charge differential.

4.3.2 Discussion

The steps shown in Fig. 19 clearly coincide with the horizontal lines. Additionally, the steps are all multiples of the smallest one. All of this leads us to state with confidence that the charge in the droplet is being changed by small multiples of single elementary charges.

The precise manipulation of charge is especially interesting for droplet collision experiments [9, 13]. If the droplets have the same polarity, they will repel each other and collisions are challenging. Another possible application would be the creation of an optical Geiger counter.

In air, the system is over-damped and, as discussed in section 2.6, the response to a displacement will follow an exponential trajectory. This can be seen in every step of Fig. 19 and a fit of a single step is shown in Fig. 20.

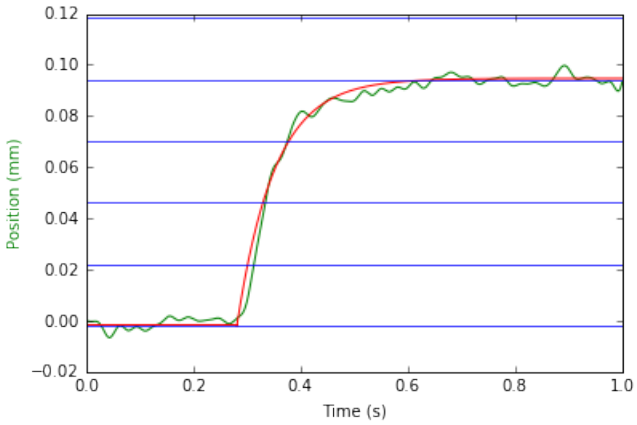

Figure 20: Over-damped harmonic oscillator return to equilibrium caused by a four electron differential (green) and the theoretical fit (red). The distance between horizontal lines represent the calculated displacement.

5 General Conclusion and Outlook

5.1 Whispering Gallery Modes

The WGM were observed during the evaporation of an optically levitated droplet and correlated to absolute measurements of the change in size. The change in droplet diameter between one WGM and the next was found to be of the same order of magnitude as the laser wavelength. Furthermore, more resonances seem to appear suggesting the existence of other resonance modes. Nevertheless, as the drop becomes smaller the effect is faster, reducing the temporal resolution of the experiment. If the effect is too fast, the droplet's movement is not fast enough and the resonances will not be visible in the change in position. A possible improvement would be to levitate the droplet using a laser with lower frequency (ej. 1064 nm). This could reduce the absorption and, therefore, the heating rate of the droplet. Moreover, a longer wavelength would increase the circumference change of the droplet needed for each resonance, thus creating a slower process with higher temporal resolution.

Regarding the evaporation process, I am very interested in measuring the temperature inside the drop. Particularly I would like to find a relationship between the temperature and the evaporation rate. The evaporation rate can already be measured extremely precisely using the WGM. A possible method to measure the temperature is to use the Raman scattering of the laser light inside the droplet, where the stokes and anti stokes peaks correlate directly to the absolute temperature inside the drop. Another important improvement would be to implement a computational program to measure the diffraction patterns of the video frame by frame and thus be able to correlate the change in size to the WGM more precisely.

5.2 Oscillation Resonances

A harmonic oscillator system was created with control over all the parameters of the DDHO differential equation. With it, the resonance effect was observed and used to calculate the trap stiffness of the system. This trap stiffness was found to be consistent with previous measurements, and the method is shown to have some advantages compared to other similar, recently published methods.

I would also like to improve the frequency sweeps in order to get a smaller uncertainty on the fitting parameters. This could be done by improving the quality of the electric field with better electrodes or by using a feedback system to stabilize the power of the laser.

I would also like to use other calibration methods to measure the trap stiffness in order to compare them with the method presented here. In particular, I would like to compare with the equipartition theorem method [28] since this one should work in vacuum, and, using Raman spectroscopy, we would have information on the drop's temperature.

5.3 Elementary Charge Differentials

A method was developed by which direct observation of the quantization of charge was achieved, creating a modern, single drop version of the Millikan experiment. Moreover, the method also provides a way to measure and manipulate the charge of the levitating droplets with elementary charge resolution.

Improvements on the droplet stability and quality of the electric field should make the step function from section 4.3 have a bigger signal to noise ratio. I would like to repeat these experiments using better electrodes and a feedback system for the laser power in order to amplify the effects.

5.4 Didactics

The two main didactic applications of this work are the DDHO in vacuum (section 4.2) and the elementary charge differentials (section 4.3).

In section 4.2, an almost ideal DDHO system was created where the damping coefficient and driving force can be manipulated by students with a knob. The transition from over- to under-damped regimes can be seen qualitatively, as shown in Fig. 12, or in the change of the amplitude-frequency graphs in Figs. 14–18. More importantly, by gradually changing the driving frequency, the resonance effect can be found empirically by students and observed with the bare eye. All of this provides a visible and manipulable example of the properties of the DDHO.

Furthermore, a demonstration like the one in section 4.3 is especially interesting for physics teaching laboratories since it compounds the possibility of observing the quantization of the electron macroscopi-

cally, and the effects of ionizing radiation. The data is recorded using a magnified image of the levitated drop. Therefore, by changing the magnification of the lens, it is possible to project the light from the droplet on a big screen and see the steps with the naked eye. A video of this was recorded [39] and could be used in a classroom.

References

[1] A. Ashkin, "History of Optical Trapping and Manipulation of Small-Neutral Particle, Atoms, and Molecules," IEEE J. Sel. Top. Quantum Electron. **6** (6), 841–856 (2000).

[2] Nobel Prize webpage physics 2018 https://www.nobelprize.org/prizes/physics/2018/summary/ .

[3] Johannes Kepler, "De Cometis Libelli III. Astronomicus ... Physicus ... Astrologicus," Aperger, 1619.

[4] J. Clerk Maxwell, "A Dynamical Theory of the Electromagnetic Field," Phil. Trans. R. Soc. Lond. **155**, 459–512 (1865).

[5] PN Lebedev, "Experimental examination of light pressure," Annalen der Physic (6) 433, (1901).

[6] Dongliang Gao, Weiqiang Ding, Manuel Nieto-Vesperinas, Xumin Ding, Mahdy Rahman, Tianhang Zhang, ChweeTeck Lim, and Cheng-Wei Qiu1, "Optical manipulation from the microscale to the nanoscale: fundamentals, advances and prospects," Light Sci. Appl. **6** (e17039), 15pp (2017).

[7] Cole D. Chapman, Kent Lee, Dean Henze, Douglas E. Smith, and Rae M. Robertson-Anderson, "Onset of Non-Continuum Effects in Microrheology of Entangled Polymer Solutions," Macromolecules, **47**, 1181–1186 (2014).

[8] Hana Šípová, Lei Shao, Nils Odebo Länk, Daniel Andrén, and Mikael Käll, "Photothermal DNA Release from Laser-Tweezed Individual Gold Nanomotors Driven by Photon Angular Momentum," ACS Photonics, **5**, 2168–2175 (2018).

[9] Maksym Ivanov, Kelken Chang, Ivan Galinskiy, Bernhard Mehlig, and Dag Hanstorp, "Optical manipulation for studies of collisional dynamics of micron-sized droplets under gravity," OPTICS EXPRESS **25** (2), 1391–1404 (2017).

[10] Bell Labs Nobel Prize in Physics 1977 https://www.bell-labs.com/about/recognition/1997-laser-trapping-atoms/ .

[11] Charles P. Blakemore, Alexander D. Rider, Sandip Roy, Qidong Wang, Akio Kawasaki, and Giorgio Gratta, "Three-dimensional force-field microscopy with optically levitated microspheres," PHYSICAL REVIEW A **99**, 023816 (2019).

[12] Akio Kawasaki, "Search for kilogram-scale dark matter with precision displacement sensors," PHYSICAL REVIEW D **99**, 023005 (2019).

[13] Albert J. Bae, Dag Hanstorp and Kelken Chang, "Juggling with Light," Phys. Rev. Lett. **122**, 043902 (2019).

[14] Alessandro Chiasera, Yannick Dumeige, Patrice Féron, Maurizio Ferrari, Yoann Jestin, Gualtiero Nunzi Conti, Stefano Pelli, Silvia Soria, and Giancarlo C. Righini, "Spherical whispering-gallery-mode microresonators," Laser and Photon. Rev. **4** (3), 457–482 (2010).

[15] A. Ashkin and J. M. Dziedzic, "Observation of Resonances in the Radiation Pressure on Dielectric Spheres," PHYSICAL REVIEW LETTERS **38** (23), 1351–1354 (1977).

[16] Thomas C Preston, Bernard J Mason, Jonathan P Reid, David Luckhaus and Ruth Signorell, "Size-dependent position of a single aerosol droplet in a Bessel beam trap," J. Opt. **16** (025702), 11pp (2014)

[17] Haesung Park and Thomas W. LeBrun, "Parametric Force Analysis for Measurement of Arbitrary Optical Forces on Particles Trapped in Air or Vacuum," ACS Photonics **2**, 1451–1459 (2015).

[18] Erik Hebestreit, Martin Frimmer, René Reimann, Christoph Dellago, Francesco Ricci, and Lukas Novotny, "Calibration and energy measurement of optically levitated nanoparticle sensors," Review of Scientific Instruments **89**, 033111 (2018).

[19] R. A. Millikan "On the Elementary Electrical Charge and the Avogadro Constant," Phys. Rev. **2**, 109–143 (1913).

[20] A. Ashkin, "Optical trapping and manipulation of neutral particles using lasers," Proc. Natl. Acad. Sci. USA **98**, 4853–4860.

[21] David C. Moore, Alexander D. Rider, and Giorgio Gratta, "Search for Millicharged Particles Using Optically Levitated Microspheres," Phys. Rev. Lett. **113** (251801), pp. 5 (2014).

[22] Martin Frimmer, Karol Luszcz, Sandra Ferreiro, Vijay Jain, Erik Hebestreit, and Lukas Novotny, "Controlling the net charge on a nanoparticle optically levitated in vacuum," Phys. Rev. A. **95**, 061801(R) pp. 4 (2017).

[23] Oscar Isaksson, Magnus Karlsteen, Mats Rostedt, and Dag Hanstorp, "An optical levitation system for a physics teaching laboratory," Am. J. Phys. **86**, 135–142 (2018).

[24] D. C. Appleyard, K. Y. Vandermeulen, H. Lee, and M. J. Langj, "Optical trapping for undergraduates," Am. J. Phys. **75**, 5–14 (2007).

[25] N. Malagnino, G. Pesce, A. Sasso and E. Arimondo, "Measurements of trapping efficiency and stiffness in optical tweezers," Optics Communications **214**, 15–24 (2002).

[26] K. F. Ren, G. Gréhan and G. Gouesbet, "Prediction of reverse radiation pressure by generalized Lorenz–Mie theory," APPLIED OPTICS **35** (15), 2702–2710 (1996).

[27] Lukas Novotny and Bert Hecht, *Principles of Nano-Optics*, Cambridge University Press, 2nd edition, 2006.

[28] M. Capitanio, G. Romano, R. Ballerini, M. Giuntini, F. S. Pavone, D. Dunlap, and L. Finzi, "Calibration of optical tweezers with differential interference contrast signals," Review of Scientific Instruments **73**, 1687–1696 (2002).

[29] Michael H. Brill, Robert C. Carter "Does Lightness Obey a Log or a Power Law? Or is That the Right Question?," Color Res. Appl. **39** (1), 99–101 (2014).

[30] Thomas R. Lettieri, Wilhelmina D. Jenkins, and Dennis A. Swyt, "Sizing of individual optically levitated evaporating droplets by measurement of resonances in the polarization ratio,", Appl. Opt. **20** (16), 2799–2805 (1981).

[31] Jan Gieseler, Bradley Deutsch, Romain Quidant, and Lukas Novotny"Subkelvin Parametric Feedback Cooling of a Laser-Trapped Nanoparticle," Phys. Rev. Lett. **109** (103603), pp. 5 (2012)

[32] A. Ashkin, and J. M. Dziedzic, "Optical levitation in high vacuum," Appl. Phys. Lett. **28**, 333–335 (1976).

[33] James A. Lock, Gérard Gouesbet, "Generalized Lorenz–Mie theory and applications," Journal of Quantitative Spectroscopy and Radiative Transfer **110**, 800–807 (2009).

[34] E. James Davis, Gustav Schweiger, *The Airborne Microparticle: Its Physics, Chemistry, Optics, and Transport Phenomena*, 1st ed. (Springer-Verlag Berlin Heidelberg, 2012), pp. 8–9.

[35] Check appendixes in the lab journal or in the lab computer: /Documents/Javier

[36] Punam Thakur and Anderson L. Ward, "Sources and distribution of 241Am in the vicinity of a deep geologic repository," Environmental Science and Pollution Research **26**, 2328–2344 (2019).

[37] The Lund/LBNL Nuclear Data Search Version 2.0, February 1999, S.Y.F. Chu, L.P. Ekström, and R.B. Firestone. nucleardata.nuclear.lu.se/toi/

[38] Henrik Andersson, *Position Sensitive Detectors - Device Technology and Applications in Spectroscopy*, Mid Sweden University Doctoral Thesis 48, pp. 20 (2008).

[39] To be made available in a future publication.

Acknowledgements

There are so many people that helped me along the way, that I will mention them in a list. I would like to thank...

- Professor Dag Hanstorp for welcoming me into his lab, for the great critiques of everything I wrote, for listening to all my crazy ideas, and for making sure I don't stray too far with them.
- Oscar Isaksson for making Mondays awesome, for telling me that it shouldn't be easy and for teaching me lagom.
- Dr. Remigio Cabrera for trusting me and sending me to Gothenburg in the first place.
- Mina, Paru and José for being part of my Gauss Curve. Specially José for being a great room-mate.
- Niels Giesselmann for his work on the setup before me.
- Jacob, Ludi, Janne and Jessica for the coffee breaks and laughs. Also to Ludi for making sure I had my pasta/rice and tuna every lunch.
- Laura and Adriana for bringing a little piece of Mexico all the way here.
- My room-mates Euriel, Sara, Sydney, Alessandra, Franz, Anton, Roberta and Robert for being my second family in Gothenburg.
- Gio for always holding on to that red string.
- My actual family in Mexico for always being ready to help, even when I didn't ask.
- The Linnaeus-Palme Foundation for making all this possible.
- And specially, to my mom, Gina, for absolutely everything else.